arXiv:1608.00436v1 [cond-mat.soft] 1 Aug 2016

Nanocapillary adhesion between parallel plates

Shengfeng Cheng[1,*] and Mark O. Robbins[2,†]

[1]*Department of Physics, Center for Soft Matter and Biological Physics, and Macromolecules Innovation Institute, Virginia Polytechnic Institute and State University, Blacksburg, Virginia 24061, USA*

[2]*Department of Physics and Astronomy, Johns Hopkins University, 3400 N. Charles Street, Baltimore, Maryland 21218, USA*

(Dated: August 2, 2016)

Molecular dynamics simulations are used to study capillary adhesion from a nanometer scale liquid bridge between two parallel flat solid surfaces. The capillary force, F_{cap}, and the meniscus shape of the bridge are computed as the separation between the solid surfaces, h, is varied. Macroscopic theory predicts the meniscus shape and the contribution of liquid/vapor interfacial tension to F_{cap} quite accurately for h as small as 2 or 3 molecular diameters (1-2 nm). However the total capillary force differs in sign and magnitude from macroscopic theory for $h \lesssim 5$ nm (8-10 diameters) because of molecular layering that is not included in macroscopic theory. For these small separations, the pressure tensor in the fluid becomes anisotropic. The components in the plane of the surface vary smoothly and are consistent with theory based on the macroscopic surface tension. Capillary adhesion is affected by only the perpendicular component, which has strong oscillations as the molecular layering changes.

PACS numbers: 68.03.Cd, 68.08.Bc, 68.08.De, 68.35.Np

I. INTRODUCTION

Capillary adhesion from liquid bridges between solids allows us to build sandcastles, enables insects to stick on a ceiling, and causes granules to agglomerate.[1–5] Condensation induced capillary adhesion is common whenever hydrophilic surfaces are in a humid environment[6, 7] and is a major cause of failure in microelectromechanical systems.[2, 8] Like other interfacial forces, capillary adhesion grows in importance as dimensions shrink to molecular scales. However capillary forces are typically modeled using macroscopic theory that must fail in the same limit.[9] In this paper we use molecular dynamics (MD) simulations to explore molecular scale changes in capillary adhesion in a simple geometry, a liquid bridge between parallel plates.

Macroscopic theory describes capillary forces in terms of two contributions.[9, 10] One is due to the surface tension from the interface of the drop (Fig. 1). The second comes from the area times the Laplace pressure in the drop due to the curvature of the interface. As dimensions shrink to nanometer scales, both terms may become inaccurate due to the finite width of the interface, changes in surface tension, changes in meniscus geometry or other new phenomena.

Some previous research attempts to identify the limits of macroscopic equations of capillarity at small length scales.[11–17] For example, it was shown that the Kelvin equation of capillary condensation, which relates the pressure difference across a liquid/vapor interface to the vapor pressure, is obeyed by cyclohexane and water menisci with a mean radius of curvature as small as 4 nm.[11–14] The Young-Laplace equation, which relates the the pressure difference between the liquid and vapor phase to the interfacial tension and the mean curvature of the interface, is found to be valid down to a similar scale.[15–17] However, it is not obvious if macroscopic theory can describe capillary forces due to liquid menisci spanning small gaps between solid surfaces, such as nanoscopic slits in porous media and granular materials or between a probe and a solid surface.

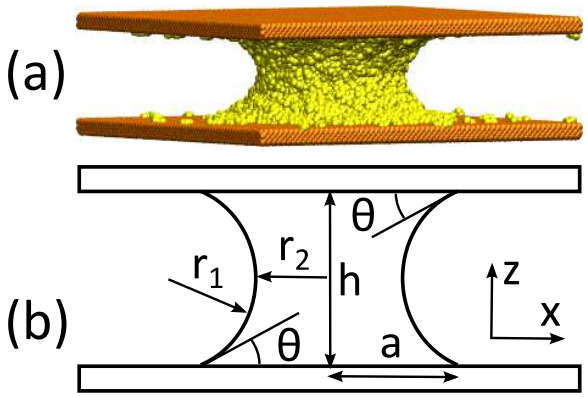

FIG. 1: (a) A liquid bridge (yellow) connects two parallel atomically flat plates (orange). (b) Geometry is specified by the contact angle θ and the radius a of the contact line at which the bridge intersects with the plates. The radius of curvature is negative (positive) when the liquid/vapor interface bends outward (inward) in the plane of curvature, as illustrated for r_1 (r_2).

In a previous paper we used molecular dynamics (MD) simulations to study the capillary adhesion in-

*Electronic address: chengsf@vt.edu
†Electronic address: mr@jhu.edu

duced by a liquid bridge between a spherical tip and a flat substrate.[18] At small separations the capillary force (F_{cap}) became progressively less attractive than predicted by macroscopic theory and oscillated rapidly with surface separation h. Analysis of the local pressure showed that these oscillations were due to layering of molecules. The layered structure led to an anisotropic pressure-stress tensor. The normal pressure component determines the term in F_{cap} from the integral of pressure over area. It developed rapid fluctuations superimposed on a gradual decrease in adhesion that explained the deviations from macroscopic theory. The in-plane component remained consistent with macroscopic theory as did the detailed shape of the meniscus. However it was difficult to probe the interfacial contribution in very narrow gaps because this work used a sphere on flat geometry. The separation between solids approached molecular scales in the center of the drop, but increased significantly by the outer meniscus. A better test of the interfacial contribution to F_{cap} requires a different geometry.

In this manuscript we consider the case of two parallel plates that sandwich a liquid bridge in a uniform gap. This geometry allows us to further check the limits of the macroscopic capillary theory based on the Young-Laplace equation. Figures 1(a) and (b) show a snapshot and a sketch of the system. This geometry approximates experiments where a small meniscus is trapped between two surfaces with very large radii of curvature. Examples include the gap between a blunt tip and a flat surface, between two large granular particles, or between two cross-aligned mica surfaces in a Surface Force Apparatus (SFA). Such geometries are of growing technological relevance because of the important role played by fluid bridges and joints in micro- and nanosystems that may arise from condensation, excretion, or trapping of liquid.[19]

As in our previous study we find that deviations from macroscopic theory are predominantly due to changes in the normal pressure caused by molecular layering. The interfacial contribution remains consistent with macroscopic theory down to gaps that are only 4 atoms across. At still smaller scales the capillary force becomes more attractive because the interface has too few atoms to approximate the predicted curvature of the meniscus. However the in-plane component of the pressure tensor continues to follow macroscopic theory to the smallest scales studied.

In the next section we provide a brief description of the simulation technique, followed by the equations of macroscopic theory. The following section presents our results for different contact angles and gaps. We end with a summary and conclusions.

II. METHODS

A. Computational model

Since our goal is to address generic behavior, we use simple potentials that have been shown to capture many aspects of the behavior of short chain molecules and polymers.[18, 20–25] Fluids are modeled as linear chains of 4 spherical beads. All beads interact with a truncated Lennard-Jones (LJ) potential

$$V_{\rm LJ}(r) = 4\epsilon \left[(\sigma/r)^{12} - (\sigma/r)^{6} - (\sigma/r_c)^{12} + (\sigma/r_c)^{6} \right] . \quad (1)$$

where ϵ is the interaction energy, σ the molecular diameter, and r_c the cutoff length. For beads not directly bonded, $r_c = 2.2\sigma$. For two neighboring beads in a chain molecule, in addition to a purely repulsive LJ interaction (i.e., $r_c = 2^{1/6}\sigma$), a finitely extensible nonlinear elastic (FENE) potential

$$V_{\rm FENE}(r) = -\frac{1}{2} K R_0^2 \ln \left[1 - (r/R_0)^2 \right] , \quad (2)$$

with the canonical values $R_0 = 1.5\sigma$ and $K = 30\epsilon/\sigma^2$ is used to describe the bonded interaction.

The LJ interaction energy ϵ, bead diameter σ, and mass m are used to define all units. To map the results to real units we use the facts that a typical hydrocarbon has molecular diameter $\sigma \sim 0.5$ nm and surface tension $\gamma = 25$ mN/m. Since the liquid/vapor interfacial tension computed in simulations is $\gamma = 0.88\epsilon/\sigma^2$, we find $\epsilon \sim 7 \times 10^{-21}$ J. Beads typically correspond to a small cluster of atoms[20] with mass $m \sim 10^{-25}$ kg. Then the characteristic LJ time, $\tau = \sqrt{m\sigma^2/\epsilon}$, is ~ 2 ps. The unit of force is $\epsilon/\sigma \sim 14$ pN and the unit of pressure $\epsilon/\sigma^3 \sim 56$ MPa.

We performed MD simulations using the LAMMPS package.[26] The equations of motion are integrated with a time step of 0.005τ. Constant temperature is maintained using a Langevin thermostat with time constant 1.0τ. For the results presented below $T = 0.75\epsilon/k_{\rm B}$, where $k_{\rm B}$ is the Boltzmann constant. This temperature is intermediate between the temperature $1.0\epsilon/k_{\rm B}$ typically used for melt simulations[20] and the glass transition temperature $\sim 0.4\epsilon/k_{\rm B}$.[23, 27] Given our estimate of ϵ, the temperature $0.75\epsilon/k_{\rm B}$ maps to a reasonable value of ~ 360K. Lowering the temperature to $0.5\epsilon/k_{\rm B}$ did not change the trends reported below but did increase the degree of layering and the magnitude of force oscillations.

For simulations reported here, the plates are treated as rigid bodies. We found that including elasticity had a negligible effect[18] because any deformation of the solids is much less than σ for elastic moduli typical of molecular solids. [a] Each plate is modeled as an fcc crystal with

[a] Elastomers have smaller moduli but also a much more complicated local structure than that considered here.[28, 29]

a (001) surface and number density $1.0\sigma^{-3}$. The fluid beads interact with the solid atoms via a LJ potential with modified interaction energy ϵ_{fs}, length scale $\sigma_{fs} = 1.2\sigma$, and cutoff $r_{cfs} = 2.16\sigma$. The interaction strength ϵ_{fs} was varied to control the contact angle θ, which was calculated by placing a drop on the plate and fitting the equilibrated drop shape to a spherical cap.[18] We found $\theta = 75^\circ$ for $\epsilon_{fs} = 0.8\epsilon$, while θ is reduced to 12° when ϵ_{fs} is increased to 1.08ϵ. We confirmed that any effects due to line tension are negligible.[18, 30]

Care must be taken in defining the plate separation that corresponds to macroscopic theory. We define h_a as the distance between the closest atoms on the surfaces of the opposing solid plates. This overestimates the volume available to the fluid because of the steric repulsion between fluid and solid atoms. To determine the effective width h_{ex} of the excluded volume near each plate we performed simulations of a fluid that contains N molecules and fills the space between two parallel solid plates of area A at zero pressure. The value of h_a should give an accessible thickness $h \equiv h_a - 2h_{ex}$ equal to that expected for the bulk density ρ_b at zero pressure: $h = h_a - 2h_{ex} = N/(A\rho_b)$. We found $h_{ex} = 0.775\sigma$ for $\epsilon_{fs} = 0.8\epsilon$ and h_{ex} decreases to 0.710σ for $\epsilon_{fs} = 1.08\epsilon$. Below we use h as the separation but the value of h_a differs only by a constant offset for a given ϵ_{fs}.

To form a liquid bridge, a drop was initially deposited on the surface of the bottom plate and allowed to relax to its equilibrium configuration. Then the top plate was brought down to contact the drop, creating a liquid bridge between the two plates. For the small contact angle shown in Fig. 1(a), a few of the molecules escape along the surface when the meniscus forms. The number remains small ($< 0.3\%$) and the vapor pressure is so low that no molecules evaporate. This justifies the use of a constant volume (V_l) ensemble in comparing macroscopic theory to simulation results. We have studied bridges with various volumes and all show similar trends. In this report we focus on a bridge with $9,316$ molecules (37,264 beads). This corresponds to $V_l = 4.123 \times 10^4\sigma^3$ at the equilibrium bulk density at zero pressure, $\rho_b = 0.904\sigma^{-3}$. There are small changes in density and volume with Laplace pressure that can be included in macroscopic theory. For the largest pressures found here ($\sim 0.5\epsilon/\sigma^3$) the changes in density are at most 1%, leading to changes in the predicted F_{cap} of the same order.

The separation between plates was varied in small steps. After each step, the liquid bridge was allowed to relax for at least 2000τ before the local and global forces were calculated. The equilibration time of the liquid bridge was less than 1000τ for $h \gtrsim 2\sigma \sim 1$ nm, and we found negligible hysteresis in the forces.[18] Hysteresis between increasing and decreasing separations was only found when $h < 2\sigma$ and the film was in a glassy state. For this reason we only present results for $h \gtrsim 2\sigma$ where the liquid bridge has reached equilibrium.

B. Macroscopic theory of capillary forces

In the macroscopic theory of capillary phenomena, the shape of the liquid bridge is determined by the Young-Laplace equation.[9] A sketch of the geometry is shown in Fig. 1(b). The interface must intersect the plates at the equilibrium contact angle θ given by Young's equation and obey the Young-Laplace equation for the local pressure change Δp across the curved interface

$$\Delta p = \gamma(1/r_1 + 1/r_2) \equiv 2\gamma\overline{\kappa} \ , \tag{3}$$

where r_i are the principal radii of curvature and $\overline{\kappa}$ is the mean curvature. The radius is positive (negative) when the center of the circle that touches the interface is inside (outside) the bridge. In Fig. 1(b) r_1 is negative. The in-plane radius r_2 is always positive.

Since gravity is negligible for nano-sized liquid bridges, Δp and thus $\overline{\kappa}$ must be constant for a given bridge. For nonvolatile liquids, Δp is fixed by the volume V_l of the bridge. For volatile liquids, Δp is determined by the relative humidity of the vapor via the Kelvin equation.[9] The results reported here are for a nonvolatile liquid because the liquid composed of chain molecules evaporates extremely slowly.[31] Results for volatile liquids are the same for a given V_l and h, but have different variations with h since V_l changes.

The capillary force has two terms in the macroscopic theory,[9, 10]

$$F_{cap} = -2\pi a\gamma \sin\theta + \pi a^2 \Delta p \ , \tag{4}$$

where a is the radius of the contact circle at which the bridge intersects with the solid surface. Our sign convention is that negative (positive) values correspond to attractions (repulsions). The first term is the vertical projection of the surface tension force and is always attractive, since moving the solid surfaces closer reduces the area of liquid/vapor interface and thus the surface free energy. This term is referred to below as F_s. The second term is the integral of the Laplace pressure over the circle where the fluid contacts the solid. This term can be either attractive or repulsive, depending on the sign of Δp, and is designated as F_p.

Equation (3) can be solved exactly using elliptic integrals.[32] The resulting continuum predictions for the shape of the bridge, F_s, F_p, and F_{cap} are then compared to MD results for the same θ and V_l.

III. RESULTS AND DISCUSSION

Within statistical fluctuations, droplets have the circular shape expected from symmetry and predicted by macroscopic theory. Figures 2(a)-(d) show the angle-averaged density profile $n(\rho, z)$ as a function of height and radial distance ρ from the center of the bridge. In all cases, there are clear oscillations in n with height that

reflect layering in the film.[18, 33–38] The LJ potential favors a spacing of order σ_{fs} between solid and fluid atoms. A sharp solid wall induces a layer of fluid at the equilibrium spacing. This layer then induces a second layer at the equilibrium spacing between fluid beads. Past studies of homogeneous thin films without menisci show that layers decay exponentially with height.[18, 33–38] The same behavior is evident in Figs. 2(a)-(d) at small ρ. There are always large oscillations in density near the wall, but this layering only spans the entire film for panels (b) and (c) where $h < 8\sigma$.

The interfaces of the drops in Figs. 2(a)-(d) are broadened by molecular discreteness and thermal fluctuations. At each z, the width of the interfacial region where n changes is comparable to molecular dimensions and a horizontal 2σ scale bar is included for reference. Also shown in Figs. 2(a)-(d) is the macroscopic prediction for the interface shape (red dashed lines). Even at the smallest wall spacings the macroscopic predictions follow the interfacial region and lie within the range where n is decaying rapidly with ρ.

To make a more precise determination of the interfacial shape and width we analyzed the decay in $n(\rho, z)$ with increasing ρ. Results were averaged over a height range comparable to the period of density oscillations, $\Delta z \sim 0.8\sigma$, because $n(\rho, z)$ drops to nearly zero at some heights near the wall. At small ρ, the density has a nearly constant value of $n_0(z)$. As ρ increases through the interfacial region, $n(\rho, z)$ drops to zero. There is no unique definition for the interface position within the interfacial region,[9] but a reasonable choice is the radius where $n(\rho, z) = 0.5n_0(z)$. Values were obtained by fitting to a common analytic form for liquid-vapor interfaces,[39] $n(\rho, z) = \frac{1}{2}n_0(z)(1 - \tanh\frac{\rho-\rho_I}{\sqrt{2}\xi})$, where ρ_I is the interface location and ξ the interface half-width at a given z. Values of the halfwidth were in the range $\xi = 1.2 \pm 0.4$ and depended on both h and z. As shown in previous work, ξ reflects both an intrinsic interface halfwidth and an additional broadening from thermal fluctuations.[40, 41]

Circles in Figs. 2(e)-(h) show the interface position ρ_I at heights corresponding to the centers of layers near the wall or in central regions where n is nearly independent of height. Red lines show the corresponding macroscopic prediction. In both cases ρ_I is referenced to the radius at the center of the film ρ_c. In all cases studied, the shapes of the interface from simulations and macroscopic theory are consistent within statistical fluctuations, which are indicated by the radii of circles ($\sim 0.1\sigma$). Thus the curvatures that enter the Laplace equation for the pressure are accurately predicted by macroscopic theory. One caveat is that the number of layers where the interface is defined decreases as h is reduced. Effects from this discreteness at $h < 4\sigma$ are noted below.

Figures 3(a) and (d) show F_{cap} vs. h for $\theta = 75°$ and $\theta = 12°$, respectively. In both cases good agreement is found between the simulations and continuum predictions for $h \gtrsim 8\sigma \sim 4$ nm. As h decreases below 8σ, pronounced oscillations in F_{cap} become apparent. These

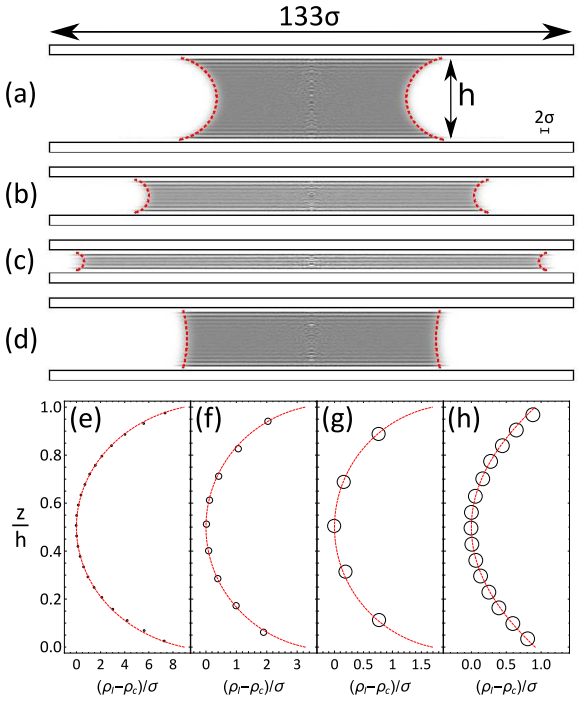

FIG. 2: Comparison of the interfacial shape from simulations and macroscopic theory (dashed red lines) for $\theta = 12°$ at (a,e) $h = 19.9\sigma$, (b,f) $h = 7.9\sigma$, (c,g) $h = 4.1\sigma$ and for $\theta = 75°$ at (d,h) $h = 13.7\sigma$. In (a)-(d) the angular averaged density $n(\rho, z)$ is represented by a gray scale plot. A horizontal scale bar indicates a width of 2σ. In (e)-(h), circles indicate the interface position ρ_I relative to the radius at the center of the meniscus ρ_c.

oscillations reflect molecular layering in the gap between plates.[18, 33–37, 42] As noted above, layering is evident in Fig. 2 and clearly spans the film for $h < 8\sigma$.

Similar oscillating forces were first observed in SFA experiments[43, 44] and later found in atomic force microscopy measurements.[45, 46] However in these experiments the entire space was filled with fluid and the oscillations represent a variation in the free energy of the film as a function of thickness rather than the capillary force. The derivative of the free energy per unit area with respect to thickness is called the disjoining pressure and its integral over the solid surfaces gives the net force between surfaces in analogy to the pressure contribution in Eq. 4.

Forces induced by molecular layering are attractive when h is close to but larger than an integral multiple of the equilibrium layer spacing because the free energy is lowered by decreasing the spacing. The force becomes repulsive when h is reduced below the optimal spacing and becomes attractive again when a layer of molecules is pushed out and h approaches the next integral number of layer spacings (see the inset of Fig. 5 below). This cycling process leads to the oscillating behavior of F_{cap} as shown in Figs. 3(a) and (d).

In the macroscopic theory, F_{cap} is the sum of the sur-

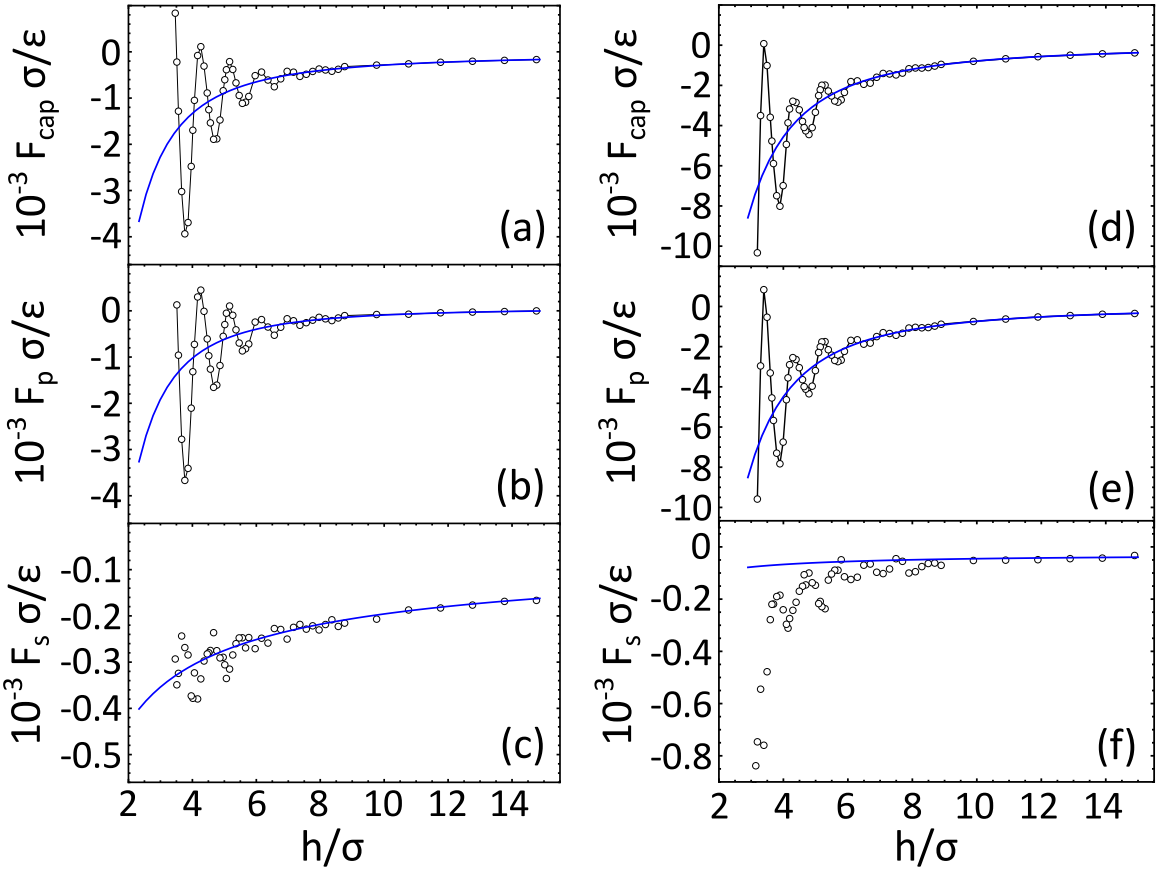

FIG. 3: Capillary forces vs. h: (a) and (d) total force; (b) and (e) contribution from the Laplace pressure; (c) and (f) contribution from the liquid/vapor surface tension. (a)-(c) are for $\theta = 75°$ and (d)-(f) for $\theta = 12°$, respectively. Blue curves represent the corresponding continuum predictions. Lines connecting data points are guides for the eye.

face tension term F_s and the pressure term F_p. To separate the two terms in simulations, we examine the vertical component of the local force between the fluid and solid atoms as a function of the lateral distance ρ from the center of the bridge. The integral F_z within a circle of radius ρ is plotted against the circle's area $\pi\rho^2$ in Fig. 4 to reduce noise from thermal fluctuations. The linear relationship between the total force and area at small ρ indicates a uniform normal pressure at the solid-liquid interface that determines F_p. Near the contact line the integral drops below this linear slope, reflecting the attractive contribution F_s from the surface tension of the liquid/vapor interface.

Linear fits like those in Fig. 4 allow us to extract a slope corresponding to the normal pressure $P_n = \frac{1}{\pi}\frac{\partial F_z}{\partial \rho^2}$ inside the liquid bridge. Note that P_n changes vary rapidly with h. In both examples shown, decreasing h by 0.1σ changes P_n by more than $0.2\epsilon/\sigma^3$. This changes the sign of the force for $\theta = 75°$. The background attraction is stronger for $\theta = 12°$, but the the magnitude of P_n decreases by about a factor of 2. The oscillations in P_n increase as h decreases and make the net force repulsive for $\theta = 12°$ at $h \simeq 3.4\sigma$ (Fig 3(d)).

The pressure contribution to F_{cap} is obtained as $F_p = \pi a^2 P_n$ where a is the radius of the contact circle. We calculated a directly from the area where wall and fluid atoms interact and also from macroscopic theory. As expected from Fig. 2, the two values agreed within less than 1% in all cases and we use the theoretical value in all the results presented below. The surface tension term is then computed as the remaining force $F_s = F_{cap} - F_p$.

Figures 3(b) and (c) show F_p and F_s as a function of h for $\theta = 75°$. The results for $\theta = 12°$ are included in Figs. 3(e) and (f). For both θ, the pressure term (F_p) agrees with the continuum curve for $h > 8\sigma \sim 4$ nm. At smaller h, F_p oscillates about the continuum solution and the magnitude of deviations grows as h decreases. These oscillations are very similar to those found in the total force. They account for almost the entire deviation from macroscopic theory because $F_s = F_{cap} - F_p$ is very close to the continuum prediction down to $h < 4\sigma$. For $\theta = 75°$ the discrepancies in F_s at small h are within numerical uncertainties because F_s is calculated as the difference between two much larger oscillating quantities and depends on the exact contact radius used. For $\theta = 12°$ there is a systematic increase in attraction at $h < 4\sigma$.

The success of continuum expressions for F_s is consistent with the agreement between the predicted and sim-

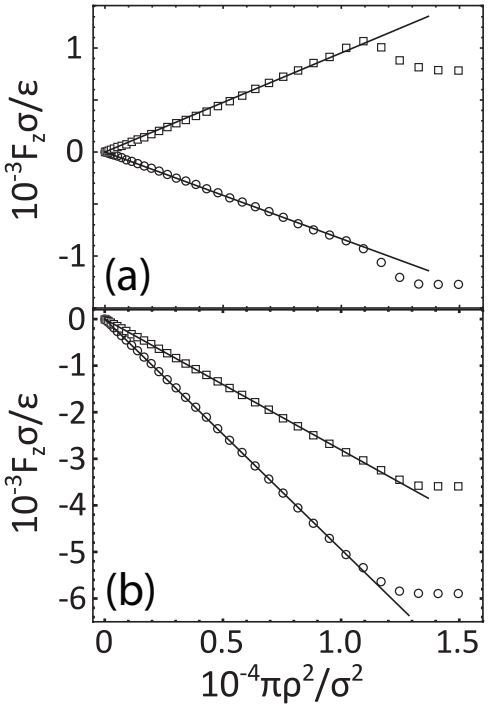

FIG. 4: The integral of the vertical force F_z within a circle of radius ρ vs. $\pi\rho^2$ at $h_a = 5.1\sigma$ (◯) and 5.0σ (□) for (a) $\theta = 75°$ and (b) $\theta = 12°$. Each linear fit gives a slope equal to the normal pressure P_n.

ulated shapes of the liquid bridge (i.e. Fig. 2) and our previous results for sphere on flat geometries.[18] Clearly the magnitude of the interfacial tension remains equal to the bulk value even in menisci that are only two or three molecules across. The increase in the magnitude of F_s for $\theta = 12°$ at $h < 4\sigma$ can be understood as a geometric effect. Macroscopic theory predicts a radius of curvature $|r_1| \approx h/(2\cos\theta)$. For $\theta = 75°$ this is much larger than h. For $\theta = 12°$, $|r_1| \approx h/2$ and as noted in discussing Fig. 2 it is not possible for the interface position at a few discrete layers to closely approximate the predicted circle. Indeed, for a two layer system the interface is always nearly vertical, leading to a capillary force proportional to γ instead of $\gamma\sin\theta$. This only changes the predicted F_s by about 4% for $\theta = 75°$, but increases the magnitude of F_s by a factor of almost 5 for $\theta = 12°$. This provides a quantitative explanation of the changes in Fig. 3(f).

It may be surprising that the fluid pressure from macroscopic theory gives the right interfacial shape from Eq. 3 but is inconsistent with the pressure that determines F_p. The resolution is that the pressure tensor becomes anisotropic at small h. The curvature of the interface is predominantly determined by the in-plane component $P_{\rho\rho}$, which remains consistent with macroscopic theory and isotropic within the plane of the plate. The normal pressure P_{zz} determines F_p. For large h the pressure is hydrostatic and $P_{zz} = P_{\rho\rho}$. This symmetry is broken as h decreases. Layering leads to strong oscillations in P_{zz} with h, but does not affect $P_{\rho\rho}$.

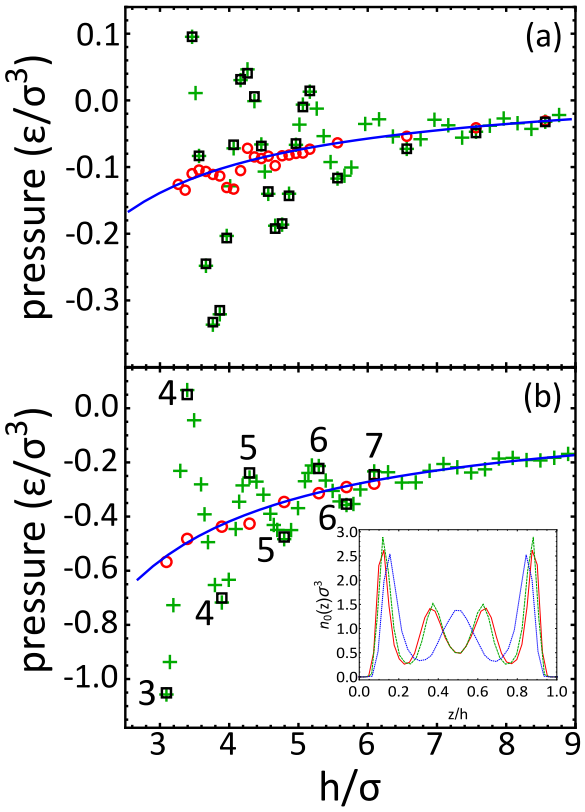

FIG. 5: Variation of the pressure tensor with plate separation for (a) $\theta = 75°$ and (b) $\theta = 12°$. The directly calculated in-plane component $P_{\rho\rho}$ (red ◯) and out-of-plane component P_{zz} (black □) of the pressure tensor are compared to P_n (green +) from the linear fits in Fig. 4 and the continuum prediction of the Laplace pressure Δp (blue solid line). Integers in (b) indicate the number of layers at local minima and maxima in P_{zz}. The inset shows density profiles at the extrema associated with 4 and 3 layers at $h = 3.9\sigma$ (red solid line), 3.4σ (green dashed line), and 3.1σ (blue dotted line).

Figure 5 shows direct evaluations of the local pressure tensor inside the liquid bridge using an algorithm proposed by Todd et al. [47]. Equivalent results were obtained with a different algorithm described by Denniston and Robbins.[40, 48] Note that the radial, in-plane component $P_{\rho\rho}$ follows the continuum prediction for Δp even in films as thin as $3\sigma \sim 1.5$ nm. In contrast, the normal pressure P_{zz} oscillates around the continuum prediction for Δp and the deviations increase as h decreases. These directly calculated values of P_{zz} are completely consistent with the normal stress P_n extracted from Fig. 4. [b]

The pressure anisotropy reflects the influence of surfaces on the liquid under confinement. The layered struc-

[b] Note that while P_{zz} oscillates with h, it is independent of height for a given h. This is required for any system in equilibrium.

ture induced by the surface leads to oscillations with h in the free energy and disjoining pressure that are not present in macroscopic theory. These lead to the oscillations in normal pressure with h in Fig. 5. For both values of θ the oscillations become large enough to change the magnitude of the force by a factor of 2 or change the force from attractive to repulsive.

The changes in layering are illustrated in Fig. 5(b). Minima and maxima in the pressure are labelled with the corresponging number of layers. At each minimum, the spacing is larger than the optimal spacing for the corresponding number of layers and there is an extra attraction pulling the surfaces together to the optimum spacing. As h decreases to the optimal spacing, this attractive term vanishes. Compressing the layer past the optimal spacing gives a repulsive force that grows until a layer is squeezed out. The inset shows density profiles corresponding to the minimum and maximum for 4 layers and the subsequent minimum after a layer has been squeezed out to leave 3 layers.

The disjoining pressure Δp_d is present even when there is no meniscus and should only depend on the local surface separation, surface interactions, density and curvature. Since the disjoining pressure only produces a contribution to the normal pressure, we define $\Delta p_d = P_n - \Delta p$ where Δp is the continuum prediction for the Laplace pressure and is consistent with $P_{\rho\rho}$. As shown in Fig. 6, Δp_d oscillates around zero and is nearly the same for both contact angles studied here. Although different contact angles reflect different interactions with the walls, the interactions are short range. Most of the variation in free energy comes from entropic packing effects that are determined by the wall spacing (h_a) but independent of θ. This is the reason that we plot Δp_d against h_a in Fig. 6. The difference in direct interactions only appear to be important at the smallest h_a where there are roughly 3 molecular layers. In our previous study of the sphere on flat geometry, there was a repulsive shift in F_{cap} as well as oscillations. This repulsive shift is not present for flat surfaces and we conclude it reflects an extra free energy cost of changing the layered structure as the curvature of the solid sphere causes the gap width to change.

The agreement between $P_{\rho\rho}$ and macroscopic theory extends to $h = 3\sigma$. This is surprising given our finding that F_s becomes more negative due to the inability of the interface to approximate a sphere on this scale. The two results are not inconsistent because the forces that produce them act in orthogonal directions. The tangential components of the stress at the liquid/vapor interface are what contribute to F_s while changes in the component normal to the interface determine $P_{\rho\rho}$. In macroscopic models the change from zero pressure outside the drop to $P_{\rho\rho}$ within the drop is mediated by the tension in the interface. This is the only possibility when all length scales are larger than the interface width. For $h < 4\sigma$ there are direct interactions between solid atoms outside the drop and fluid atoms near the center of the meniscus that can replace the tension from the interface. Indeed these interactions lead to the tension at the contact line in a larger drop and the change in $P_{\rho\rho}$ there. This explains why the radial stress can continue to follow the macroscopic prediction even in extremely thin films.

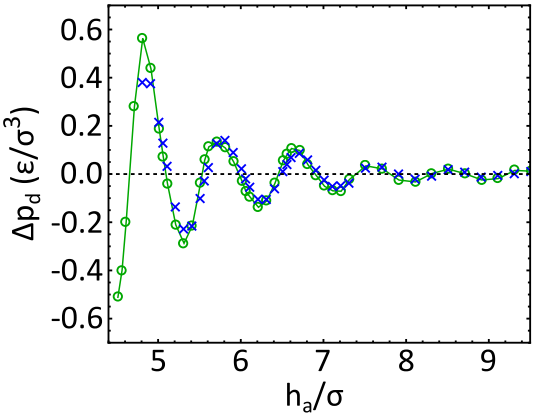

FIG. 6: The disjoining pressure ($\Delta p_d = P_n - P_{\rho\rho}$) as a function of the separation between wall atoms (h_a) for $\theta = 75^\circ$ (blue $\times$) and $\theta = 12^\circ$ (green $\bigcirc$). The lines are guides for the eye.

IV. CONCLUSIONS

The simulations presented here show that the macroscopic theory of capillarity works down to surprisingly small scales. Within statistical uncertainties ($\sim 0.1\sigma$ and 1%), the meniscus shape and forces agree with the continuum prediction down to $h \sim 8\sigma$ (~ 4 nm). Below that scale, molecular layering produces strong oscillations in the force that are not captured by macroscopic theory. The shape of the liquid bridge and the Young-Laplace equation remain accurate to even smaller scales ($h \sim$ 3-4σ).

The shape of the interface remains consistent with macroscopic theory as long as the radius of curvature is much larger than the molecular diameter. Fig. 2 shows good agreement even for $h = 4.1\sigma$ and $\theta = 12^\circ$ where $|r_1| = h/(2\cos\theta) \sim 2.1\sigma$. As h decreases further, layering introduces discreteness in the interface profile and limits the decrease in radius. In the limit of one or two layers, the radius of the interface must always be effectively independent of height, implying zero vertical curvature and $\theta \sim 90^\circ$. Since the surface tension contribution to the capillary force $F_s \propto \sin\theta$, there is a large increase in the magnitude of F_s for fluids with equilibrium angles near 0° (Fig. 3(f)) or 180°.

Detailed analysis of the local pressure tensor allowed us to isolate the trends in different contributions to the capillary force. When $h \lesssim 8\sigma$ the pressure inside the liquid bridge becomes anisotropic. The in-plane component $P_{\rho\rho}$ is consistent with the macroscopic solution for the Laplace pressure Δp for h down to 3-4σ, even when layering prevents the meniscus from following the

high predicted curvature. For these very thin films, direct interactions with the wall span the entire interface and replace the interfacial tension assumed in the Young-Laplace equation. In contrast, the normal component P_{zz} does not follow the macroscopic solution. It has an additional contribution that oscillates rapidly with h and is large enough to change the sign of the pressure as well as the magnitude.

The difference between normal and in-plane pressures, $\Delta p_d = P_{zz} - \Delta p$, represents a disjoining pressure from changes in free energy per unit area with surface separation. The oscillation period corresponds to the spacing between molecular layers that form near the walls and span the system for $h \lesssim 8\sigma$. For the short range interactions used here, Δp_d is nearly independent of changes in wall interactions that change θ from 75° to 12° (Fig. 6). This indicates that Δp_d is predominantly from entropy associated with layer packing at a given wall spacing. The disjoining pressure is nearly independent of drop volume as long as the contact radius $a >> h$.

It is useful to compare the results from the simulations presented here to those in our previous study of capillary adhesion in the sphere-on-flat geometry.[18] This earlier paper also found that macroscopic theory described the interface shape but did not study menisci with heights less than 10σ because the curvature of the sphere led to large separations at the liquid/vapor interface. The most significant difference between the two studies is that the disjoining pressure for curved surfaces always had an additional repulsive component that increased with decreasing h and sphere radius. This repulsion is not present for the flat surfaces used here. The increase in the magnitude of Δp_d with increasing curvature confirms that it represents an additional entropic cost associated with changing the number of layers as curvature changes the local separation between the surfaces.

Experiments show that the range of the disjoining pressure can vary greatly with molecular structure and interactions.[34, 35, 38, 43, 49–52] Our results suggest that the capillary force will be consistent with macroscopic theory until the disjoining pressure is significant. If the disjoining pressure is added to the macroscopic theory, the result should remain accurate until h approaches the molecular diameter or the thickness of the liquid/vapor interface. The two are the same in our system but the interface thickness may be larger, for example near a critical point. It will be interesting to test these ideas and to include the effect of surface roughness which may increase repulsion and lead to variations in the local contact angle. Studies of plates with asymmetric wetting properties would also allow tests of macroscopic predictions, such as work that finds attraction whenever the sum of the contact angles on the solid plates is less than 180 degrees.[53, 54]

Acknowledgement

This material is based upon work supported by the National Science Foundation under Grant No. DMR-1411144.

[1] Hornbaker, D. J.; Albert, R.; Albert, I.; Barabási, A. L.; Schiffer, P. What Keeps Sandcastles Standing? *Nature* **1997**, *387*, 765–765.

[2] Weiss, P. The Little Engines That Couldn't: Tired of Grinding Their Gears, Micromachine Researchers Turn to Surface Science. *Science News* **2000**, *158*, 56–58.

[3] Rabinovich, Y. I.; Esayanur, M. S.; Johanson, K. D.; Adler, J. J.; Moudgil, B. M. Measurement of Oil-mediated Particle Adhesion to a Silica Substrate by Atomic Force Microscopy. *J. Adhesion Sci. Technol.* **2002**, *16*, 887–903.

[4] Herminghaus, S. Dynamics of Wet Granular Matter. *Adv. Phys.* **2005**, *54*, 221–261.

[5] Scheel, M.; Seemann, R.; Brinkmann, M.; Michiel, M. D.; Sheppard, A.; Breidenbach, B.; Herminghaus, S. Morphological Clues to Wet Granular Pile Stability. *Nature Mater.* **2008**, *7*, 189–193.

[6] Riedo, E.; Lévy, F.; Brune, H. Kinetics of Capillary Condensation in Nanoscopic Sliding Friction. *Phys. Rev. Lett.* **2002**, *88*, 185505.

[7] Charlaix, E.; Ciccotti, M. In *Handbook of Nanophysics: Principles and Methods*; Sattler, K., Ed.; CRC Press: Boca Raton, FL, 2010.

[8] Maboudian, R.; Ashurst, W. R.; Carraro, C. Tribological Challenges in Micromechanical Systems. *Trib. Lett.* **2002**, *12*, 95–100.

[9] Rowlinson, J. S.; Widom, B. *Molecular Theory of Capillarity*; Oxford: Oxford, 1989.

[10] Lambert, P.; Chau, A.; Delchambre, A. Comparison between Two Capillary Forces Models. *Langmuir* **2008**, *24*, 3157–3163.

[11] Fisher, L. R.; Israelachvili, J. N. Direct Experimental Verification of the Kelvin Equation for Capillary Condensation. *Naturale* **1979**, *277*, 548–549.

[12] Fisher, L. R.; Israelachvili, J. N. Experimental Studies on the Applicability of the Kelvin Equation to Highly Curved Concave Menisci. *J. Colloid Interface Sci.* **1981**, *80*, 528–541.

[13] Fisher, L. R.; Gamble, R. A.; Middlehurst, J. The Kelvin Equation and the Capillary Condensation of Water. *Nature* **1981**, *290*, 575–576.

[14] Kohonen, M. M.; Christenson, H. K. Capillary Condensation of Water between Rinsed Mica Surfaces. *Langmuir* **2000**, *16*, 7285–7288.

[15] Thompson, P. A.; Brinckerhoff, W. B.; Robbins, M. O. Microscopic Studies of Static and Dynamic Contact Angles. *J. Adhesion Sci. Technol.* **1993**, *7*, 535–554.

[16] Bresme, F.; Quirke, N. Computer Simuation Study of the Wetting Behavior and Line Tensions of Nanometer Size Particulates at a Liquid-vapor Interface. *Phys. Rev. Lett.* **1998**, *80*, 3791–3794.

[17] Takahashi, H.; Morita, A. A Molecular Dynamics Study

on Inner Pressure of Microbubbles in Liquid Argon and Water. *Chem. Phys. Lett.* **2013**, *573*, 35 – 40.

[18] Cheng, S.; Robbins, M. O. Capillary Adhesion at the Nanometer Scale. *Phys. Rev. E* **2014**, *89*, 062402.

[19] Mastrangeli, M. The Fluid Joint: The Soft Spot of Micro- and Nanosystems. *Adv. Mater.* **2015**, *27*, 4254–4272.

[20] Kremer, K.; Grest, G. S. Dynamics of Entangled Linear Polymer Melts: A Molecular-Dynamics Simulation. *J. Chem. Phys.* **1990**, *92*, 5057–5086.

[21] Kröger, M.; Loose, W.; Hess, S. Rheology and Structural Changes of Polymer Melts via Nonequilibrium Molecular Dynamics. *J. Rheology* **1993**, *37*, 1057–1079.

[22] Hur, J. S.; Shaqfeh, E. S. G.; Larson, R. G. Brownian Dynamics Simulations of Single DNA Molecules in Shear Flow. *J. Rheology* **2000**, *44*, 713–742.

[23] Rottler, J.; Robbins, M. O. Shear Yielding of Amorphous Glassy Solids: Effect of Temperature and Strain Rate. *Phys. Rev. E* **2003**, *68*, 011507.

[24] Kröger, M. Simple Models for Complex Nonequilibrium Fluids. *Phys. Rep.* **2004**, *390*, 453 – 551.

[25] Cheng, S.; Luan, B. Q.; Robbins, M. O. Contact and Friction of Nanoasperities: Effects of Adsorbed Monolayers. *Phys. Rev. E* **2010**, *81*, 016102.

[26] http://lammps.sandia.gov/.

[27] Buchholz, J.; Paul, W.; Varnik, F.; Binder, K. Cooling Rate Dependence of the Glass Transition Temperature of Polymer Melts: Molecular Dynamics Study. *J. Chem. Phys.* **2002**, *117*, 7364–7372.

[28] Style, R. W.; Dufresne, E. R. Static Wetting on Deformable Substrates, from Liquids to Soft Solids. *Soft Matter* **2012**, *8*, 7177–7184.

[29] Style, R. W.; Boltyanskiy, R.; Che, Y.; Wettlaufer, J. S.; Wilen, L. A.; Dufresne, E. R. Universal Deformation of Soft Substrates Near a Contact Line and the Direct Measurement of Solid Surface Stresses. *Phys. Rev. Lett.* **2013**, *110*, 066103.

[30] Amirfazli, A.; Neumann, A. Status of the Three-phase Line Tension: A Review. *Adv. Colloid Interface Sci.* **2004**, *110*, 121 – 141.

[31] Cheng, S.; Lechman, J. B.; Plimpton, S. J.; Grest, G. S. Evaporation of Lennard-Jones Fluids. *J. Chem. Phys.* **2011**, *134*, 224704.

[32] Orr, F. M.; Scriven, L. E.; Rivas, A. P. Pendular Rings between Solids: Meniscus Properties and Capillary Force. *J. Fluid Mech.* **1975**, *67*, 723–742.

[33] Nordholm, S.; Haymet, A. D. J. Generalized van der Waals Theory. I Basic Formulation and Application to Uniform Fluids. *Aust. J. Chem.* **1980**, *33*, 2013–2027.

[34] Toxvaerd, S. The Structure and Thermodynamics of a Solid-fluid Interface. *J. Chem. Phys.* **1981**, *74*, 1998–2008.

[35] Magda, J.; Tirrell, M.; Davis, H. T. Molecular Dynamics of Narrow, Liquid-filled Pores. *J. Chem. Phys.* **1985**, *83*, 1888–1901.

[36] Bitsanis, I.; Hadziioannou, G. Molecular Dynamics Simulations of the Structure and Dynamics of Confined Polymer Melts. *J. Chem. Phys.* **1990**, *92*, 3827–3847.

[37] Gao, J.; Luedtke, W. D.; Landman, U. Layering Transitions and Dynamics of Confined Liquid Fims. *Phys. Rev. Lett.* **1997**, *79*, 705–708.

[38] Thompson, P. A.; Robbins, M. O. Shear Flow Near Solids: Epitaxial Order and Flow Boundary Conditions. *Phys. Rev. A* **1990**, *41*, 6830–6837.

[39] Jasnow, D.; Viñals, J. Coarse-grained Description of Thermo-capillary Flow. *Phys. Fluids* **1996**, *8*, 660–669.

[40] Denniston, C.; Robbins, M. O. Mapping Molecular Models to Continuum Theories for Partially Miscible Fluids. *Phys. Rev. E* **2004**, *69*, 021505.

[41] Lacasse, M.-D.; Grest, G. S.; Levine, A. J. Capillary-wave and Chain-length Effects at Polymer/Polymer Interfaces. *Phys. Rev. Lett.* **1998**, *80*, 309–312.

[42] Denniston, C.; Robbins, M. O. Matching Continuum Boundary Conditions to Molecular Dynamics Simulations for a Miscible Binary Fluid. *J. Chem. Phys.* **2006**, *125*, 214102.

[43] Horn, R. G.; Israelachvili, J. N. Direct Measurement of Structural Forces between Two Surfaces in a Nonpolar Liquid. *J. Chem. Phys.* **1981**, *75*, 1400–1412.

[44] Israelachvili, J. N.; Tirrell, M.; Klein, J.; Almog, Y. Forces between Two Layers of Adsorbed Polystyrene Immersed in Cyclohexane below and above the θ Temperature. *Macromolecules* **1984**, *17*, 204–209.

[45] Jarvis, S. P.; Uchihashi, T.; Ishida, T.; Tokumoto, H.; Nakayama, Y. Local Solvation Shell Measurement in Water Using a Carbon Nanotube Probe. *J. Phys. Chem. B* **2000**, *104*, 6091–6094.

[46] Kočevar, K.; Borštnik, A.; Muševič, I.; Žumer, S. Capillary Condensation of a Nematic Liquid Crystal Observed by Force Spectroscopy. *Phys. Rev. Lett.* **2001**, *86*, 5914–5917.

[47] Todd, B. D.; Evans, D. J.; Daivis, P. J. Pressure Tensor for Inhomogeneous Fluids. *Phys. Rev. E* **1995**, *52*, 1627–1638.

[48] Denniston, C.; Robbins, M. O. Molecular and Continuum Boundary Conditions for a Miscible Binary Fluid. *Phys. Rev. Lett.* **2001**, *87*, 178302.

[49] de Gennes, P. G. Wetting: Statics and Dynamics. *Rev. Mod. Phys.* **1985**, *57*, 827–863.

[50] White, L. R. The Contact Angle on an Elastic Substrate. 1. The Role of Disjoining Pressure in the Surface Mechanics. *J. Colloid Interface Sci.* **2003**, *258*, 82–96.

[51] Bowles, A. P.; Hsia, Y.-T.; Jones, P. M.; Schneider, J. W.; White, L. R. Quasi-equilibrium AFM Measurement of Disjoining Pressure in Lubricant Nano-films I: Fomblin Z03 on Silica. *Langmuir* **2006**, *22*, 11436–11446.

[52] Dutka, F.; Napiórkowski, M. The Influence of van der Waals Forces on Droplet Morphological Transitions and Solvation Forces in Nanochannels. *J. Phys.: Condens. Matter* **2014**, *26*, 035101.

[53] Souza, E. J. D.; Gao, L.; McCarthy, T. J.; Arzt, E.; Crosby, A. J. Effect of Contact Angle Hysteresis on the Measurement of Capillary Forces. *Langmuir* **2008**, *24*, 1391–1396.

[54] Souza, E. J. D.; Brinkmann, M.; Mohrdieck, C.; Crosby, A. J.; Arzt, E. Capillary Forces between Chemically Different Substrates. *Langmuir* **2008**, *24*, 10161–10168.